# Electron Density Fluctuation Measurements in Projectile Wakes

JAY FOX* AND HARALD RUNGALDIER†
*TRW Systems Group, Redondo Beach, Calif.*

**To understand the scattering properties of hypersonic wakes, it is necessary to have spatially resolved measurements of wake electron density fluctuation spectra. Such measurements are provided herein in the wake of sphere projectiles moving at 6 kfps in a 20-torr krypton atmosphere. Under these Mach 9 conditions, a high degree of ionization was produced and recombination chemistry was essentially frozen for long distances in the turbulent wake. To obtain the electron density measurements, three Langmuir probes were located adjacent to the projectile path, thus providing correlations and convection velocity of the fluctuations in addition to spectra. Electron density was measured in the range of $X/D$ from $10^2$ to $10^3$ using collection wires that were 0.0001 in. in diam. They were operated in the electron-saturation mode, the collisionless sheaths being large compared with the wire diameter. Using a large bias, the current was directly proportional to the local instantaneous electron density. The present measurements are believed to be the first direct electron density measurements of projectile wakes on a local and instantaneous basis that are available. Mean values of electron density near $10^{10}$/cc with peaks approaching $10^{11}$ were obtained. The rms fluctuations were 0.6 to 1.0 of the mean electron density. The spectrum of the electron density fluctuations agrees with the previously obtained anemometer data spectrum, which suggests that the electron fluctuations are acting as passive scalars in the velocity and mass-density fluctuation field.**

## Nomenclature

$A$ = area
$D$ = diameter of projectile
$D_w$ = diameter of wire
$e$ = charge of an electron
$f$ = frequency, Hz
$g, G$ = instantaneous and mean value of data
$I$ = electron collection current [Eqs. (1) and (2)]
$k$ = Boltzmann constant
$M$ = Mach number of projectile flow
$M_e$ = mass of electron
$n_e$ = electron density
$n_e'$ = rms electron density
$\overline{n_e}$ = mean electron density
$P$ = power spectrum
$t$ = time
$T$ = temperature or time
$V$ = voltage or wake velocity
$V_B$ = projectile velocity
$X$ = axial distance behind projectile
$y$ = radial distance from projectile axis
$\theta$ = time correlation integral scale
$\lambda$ = mean free path
$\lambda_D$ = Debye length
$\Lambda$ = space correlation length scale
$\sigma_2$ = standard deviation or rms [Eq. (3)]
$\sigma_3$ = third central moment [Eq. (4)]
$\sigma_4$ = fourth central moment [Eq. (5)]
$\tilde{\sigma}_4$ = modified $\sigma_4$, equals $\sigma_4 - 3$
$\tau$ = time correlation microscale

Received July 9, 1970; revision received January 31, 1972. This work was supported by ARPA/SAMSO under contracts F04701-69-C-0119 and F04701-70-C-0152. The authors acknowledge the inspiration and contributions of the late W. H. Webb.

Index categories: Jets, Wakes, and Viscid-Inviscid Flow Interactions; Plasma Dynamics and MHD; Reactive Flows.

* Staff Engineer, Re-entry Physics Department. Member AIAA.

† Member of the Technical Staff, Advanced Applications Department. Associate Member AIAA.

## Introduction

THE need for electron density measurements on a local instantaneous basis of the turbulent wakes behind hypersonic projectiles has long been recognized. Early measurement techniques used various microwave techniques which produced volume-averaged or line-integrated electron density.[1,2] Recent electrostatic probe measurements[3,4] have used continuum collection, which produces data that are dependent on temperature and velocity as well as electron density. Because the instantaneous temperature and velocity were not measured independently during those experiments, the electron density was inferred by hypothesis. This procedure leads to some degree of ambiguity, notwithstanding the recently obtained mean values of local electron density that compare well with integrated microwave results.[4] Because the present measurements are instantaneous local measurements of electron density, the mean values, rms fluctuations, and frequency spectrum of electron density fluctuations have been calculated directly from the data, a procedure which was not possible in the previous references.

## Experimental Methods

Half-inch sphere projectiles at 6000 fps were used in the experimental arrangement shown in Fig. 1. The heavy atomic weight of krypton provided the Mach 9 conditions in the monatomic gas. The high degree of ionization obtained in krypton is mainly due to the close approximation to ideal gas conditions that was obtained in the bow stagnation region of the projectile flow. Compared to air or other diatomic flows, a high-stagnation temperature for ionization was obtained because there was neither vibrational nor rotational modes to absorb energy. Krypton's ionization potential of 14 v contributes little to the high-ionization level; it is comparable with those of atomic nitrogen, oxygen, or hydrogen, which are not exceptional.

The arrangement of the experiments that is shown in Fig. 1 is similar to that used in the previous anemometer measurements.[5-7] Orthogonal shadowgraphs measured the location of

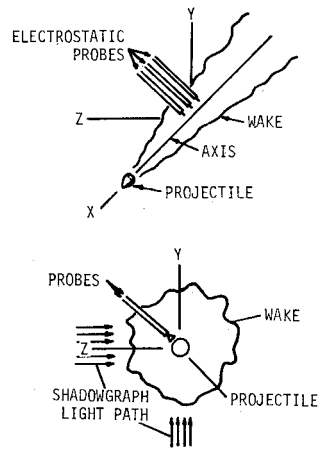


**Fig. 1 Configuration of the ballistic range experiment.**

the projectile with respect to the probes. For the 19 shots in the data reduction program, the off-axis distance of the probes ranged from 0.8 to 1.2 projectile diameters. The data were divided into three groups centered around $y/D = 0.86$, 1.05, and 1.18, when radial or off-axis studies were conducted.

The 20 mm krypton pressure of the ballistic range was the minimum for consistent turbulent wake, there being a high unit Reynolds number for krypton compared with air. The wake grew over the three probes after projectile travel of 20–40 $X/D$ and immersed the three collection wires in the turbulent electron-rich flow. For the tungsten wires, which were 0.0001 in. diameter with platinum 5 $\mu$in. coating, the classical collisionless theory with orbit-motion limiting[8] was used. The electron current collected at high-positive bias was

$$I = eAn_e(2kT/\pi^2 M_e)^{1/2}(1+eV/kT)^{1/2} \quad (1)$$

Because $(eV)/(kT) \gg 1$ was always maintained, the current was thus directly proportional to electron density $n_e$ and independent of temperature $T$, and Eq. (1) became

$$I = eAn_e(2eV/\pi^2 M_e)^{1/2} \quad (2)$$

A positive 10 v bias was used to prevent minor (about 1 v) plasma potential variations from influencing the data more than 5%. Typical wake conditions of 1500°K, 20 torr of krypton, and $n_e$ near $10^{11}$/cc gave the required conditions for the validity of Eq. (2), namely $\lambda/D_w = 10$ and $\lambda_D/D_w = 3$. Sheath diameters were about $\frac{1}{10}$ of the wire length. Collection currents up to $10^{-4}$ amp were obtained in the experiment. Recent studies of probe response in fluctuating plasmas[9,10] have verified that Eq. (2) is valid for fluctuations as well. Hence, the rms fluctuating electron density and the frequency spectrum of the electron density fluctuations were obtained from the corresponding treatment of the electron current.

Care was taken to limit the exposed area of the collection wire and avoid depleting the plasma. Likewise, large lengths of ground return wire were provided to keep the plasma potential within about 1 v of the ground. The exposed length of wire was about 0.025 in. compared with the total length of 0.100 in. The wires were suspended between the ground post and the collection post and were attached to the ground post with insulating adhesive. Soft solder completed the circuit to the collection post. The ground wires (about 30 in. long) were soldered to the ground post starting about 0.060 in. away from the collection wire and were wrapped around the insulated collection post in spaced loops leading away from the collection wire. In Fig. 1, the collection wire orientation can be seen as perpendicular to the mean wake velocity; they are supported at both ends following the suggestion of Ref. 11.

The current was measured with current-to-voltage transducers at the base of the probes. The voltage data was recorded on a DC-20 kHz FM tape recorder using two parallel channels with overlapping sensitivities for each probe. Digitizing was accomplished at the rate of 80,000 samples/sec on each channel, one data channel being digitized for each of the three probes. The analysis of the data on a digital computer was done in one-msec segments using a more comprehensive computer program than that used in previous measurements.[5-7] Probability quantities as well as correlations and spectra were calculated. In Fig. 2, sample data and probability results are shown for "spikey" and "nonspikey" data. Histograms, which collect all the points in the data segment according to the data value, are shown for the two sample cases, The histogram for the spikey sample shows that the level with the highest population of data is slightly below the mean with other levels being populated with fewer points and extending to levels well above the mean value. The nonspikey data histogram shows a more even distribution of population with levels below the mean value extending slightly further than those above it.

The data of Fig. 2 have some of the characteristics of intermittency in a restricted sense. The electrons in the wake fluctuate to a large degree, as will be shown later, and the mean gradients are large. Since the measurement locations are mostly well within the turbulent front of the wake, no special treatment of the data was made with regard to the intermittent appearance of the data.

The histograms or amplitude distribution are characterized by the central moments

$$\sigma_2{}^2 = \frac{1}{T}\int_0^T [g(t)-G(t)]^2\,dt \quad (3)$$

$$\sigma_3 = \frac{1}{T}\int_0^T [g(t)-G(t)]^3\,dt/\sigma_2{}^3 \quad (4)$$

$$\sigma_4 = \frac{1}{T}\int_0^T [g(t)-G(t)]^4\,dt/\sigma_2{}^4 \quad (5)$$

where $\sigma_2$ and $\sigma_2{}^2$ are also known as the standard deviation (or rms) and variance, respectively. The normalized third and fourth moments $\sigma_3$ and $\sigma_4$ are also known as skewness and flatness (or kurtosis), respectively. For a Gaussian distribution, $\sigma_3$ is zero and $\sigma_4$ is 3. A modified fourth moment $\tilde{\sigma}_4 = \sigma_4 - 3$ was defined for convenience in plotting comparisons.

The $\sigma_3$ and $\sigma_4$ of the sample data of Fig. 2 show some significant features of the histograms. The $\sigma_3$ for the spikey case is positive while the nonspikey case has $\sigma_3$ negative. These trends in skewness $\sigma_3$ correspond to the direction of the "tails" of the histograms leading farthest away from the mean values. The distributions of sample data are somewhat sharper than the Gaussian distribution, as measured by $\sigma_4$.

The correlations and their Fourier transforms, the power spectra, were calculated using lagged products and cosine transforms, as before.[5-7] Twenty percent of the data length in the msec segments was used for the maximum lags. The frequency resolution was 2.5 kHz, with 40 kHz being the maximum frequency of the analysis.

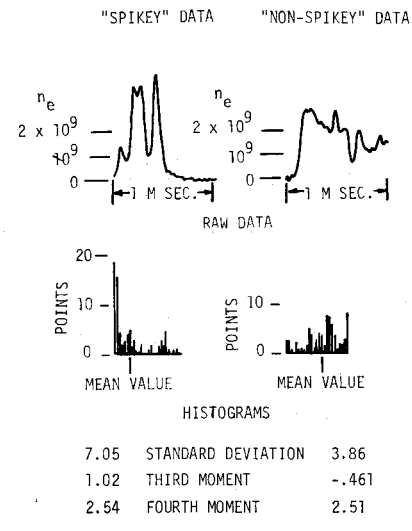


**Fig. 2 Sample data comparing spikey and nonspikey data using histograms and moments.**

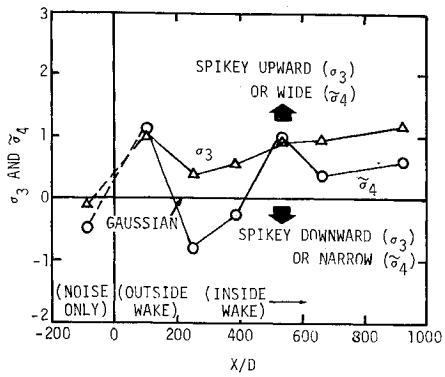


Fig. 3 Average normalized third and fourth moments showing the spikey upward nature of the wake data. Data at $X/D = 100$ are partially outside wake.

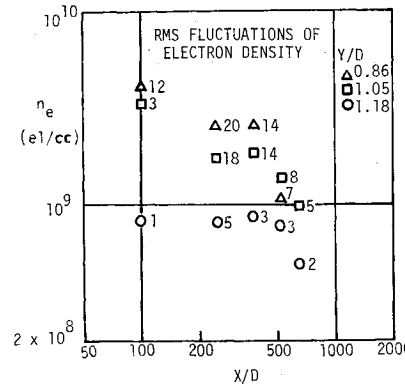


Fig. 5 rms fluctuations of electron density showing variations with axial and radial distance. Numbers are average basis.

## Probability Results

Figure 3 shows the average values of the central moments $\sigma_3$ and $\tilde{\sigma}_4$ which are both defined to be zero for a Gaussian distribution. The noise values before the projectile arrives show a nearly symmetrical distribution ($\sigma_3$ is small). At $X/D = 100$, the data are taken at the edge of the turbulent wake as the wake is growing over the probes. A large positive skewness $\sigma_3$ or spikey upwards nature to the distribution of data is shown in this low $X/D$ data; it decreases somewhat at larger $X/D$ as the wake gets larger, but $\sigma_3$ maintains positive average value throughout the wake length. The wake data are truly spikey upwards on the average like the sample spikey data in Fig. 2.

The modified flatness or width moment $\tilde{\sigma}_4$ in Fig. 3 shows some similar numerical trends compared with $\sigma_3$, but varies from wide to narrow to wide values over the length of the wake.

## Electron Density Results

The mean electron density values are shown in Fig. 4 with the numbers indicating the individual data that contribute to the average of the individual mean values. At each $X/D$ analysis location, each of the three probe data were available to contribute to the average. Depending on the signal-to-noise ratio of the data, a larger or smaller number was available for averaging. This $S/N$ ratio depended on sensitivity setting of the instrumentation, the off-axis or $y/D$ distance, and the electron density $\overline{n_e}$ at the $X/D$ location. Fewer values were available at large off-axis values and larger axial distances.

A strong radial gradient with $y/D$ in Fig. 4 is evident up to $X/D = 380$. At larger $X/D$, this radial gradient gives way to a random effect near the end of the wake at $X/D = 660$. At $X/D = 100$, the probes are at the edge of the turbulent viscous wake where the electron-rich inviscid wake is supplying electrons to the turbulent wake. Estimates of $\overline{n_e} = 10^{11}$/cc on the axis at these low $X/D$ were made before the experiment; they were based on equilibrium conditions in the bow stagnation region and suitable estimates of expansion around the body and frozen chemistry in the wake. From the data in Fig. 4, the estimates of $\overline{n_e}$ on the axis seem reasonably accurate at low $X/D$.

As the wake grows larger with $X/D$, dilution lowers $\overline{n_e}$ until the temperature of 600–800°K is reached. At this temperature, an oxygen-attachment reaction quickly cleans up the remaining electrons. Trace amounts of oxygen in the range are sufficient for this reaction because the electrons are such a small trace in the flow.

The root-mean-square (rms) fluctuations of electron density $n_e'$ shown in Fig. 5 are the first available results for fluctuations in projectile wakes, as indicated in the Introduction. The trends of $n_e'$ have roughly the same trends and magnitudes as the $\overline{n_e}$ shown in Fig. 4; both the $y/D$ and $X/D$ trends are similar. An interesting feature is the data at $X/D = 100$, where the fluctuations are being observed when the probes are partially outside the turbulent wake. The probes are still inside the inviscid wake with its steep electron density gradient. Evidently, the acoustic-mode propagation of turbulence from the inside turbulent core of the wake causes disturbances in the inviscid wake at the probe location. Small movements in that flow with its steep $\overline{n_e}$ gradient cause a turbulent signal to be read by the probe. These data will be shown later to have a turbulent spectrum.

The ratio $n_e'/\overline{n_e}$, which is known as electron density fluctuation intensity, is shown in Fig. 6 for the range of $X/D$ from 100 to 660. The values of $n_e'/\overline{n_e}$ are individually plotted for the three $y/D$ locations that showed trends for the $n_e'$ and $\overline{n_e}$. However, the intensity $n_e'/\overline{n_e}$ shows no trend with $y/D$ nor $X/D$, but rather a scatter of data generally between 0.6 and 1.0.

## Correlation Results

Convection velocity results are shown in Fig. 7. For this

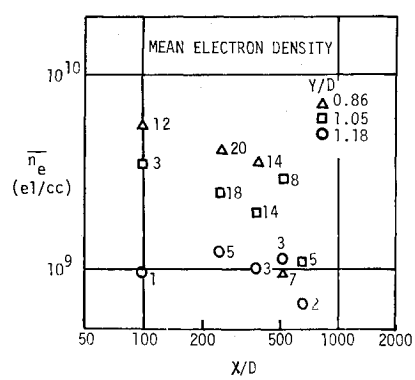


Fig. 4 Mean electron density showing variation with axial and radial distance. Numbers with data symbols indicate number contributing to average value.

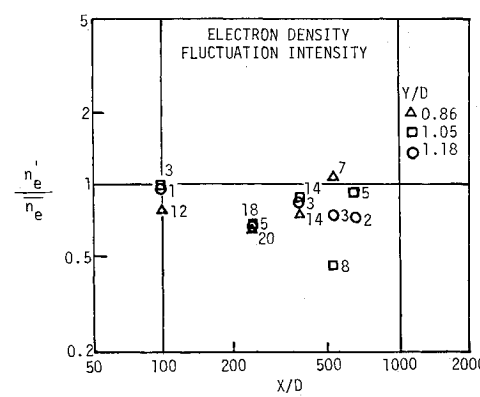


Fig. 6 Electron density fluctuation intensity showing comparison with value from Lees-Hromas-Webb theory. Numbers are average basis.

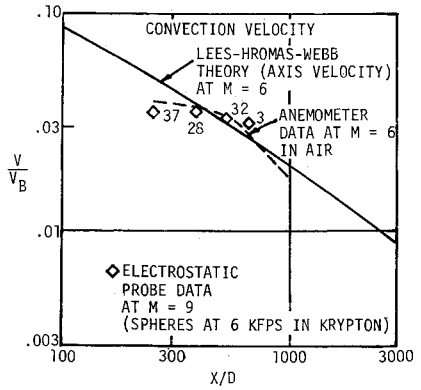


**Fig. 7 Convection velocity ratio. Comparison of axial trends with anemometer data and also with Lee-Hromas-Webb theory.**

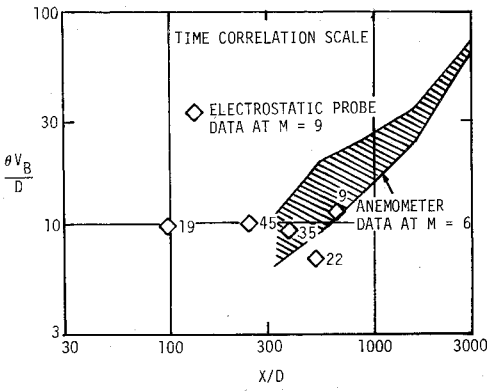


**Fig. 9 Time correlation integral scale compared with anemometer data.**

measurement, the fluctuating electron density data from the three possible pairs of probes were cross correlated and the delay time to the best cross correlation was determined. This time is the average transit time or convection time of a fluctuation embedded in the flow to travel from one probe to the other. This convection time was averaged between shots and used to determine the convection velocity based on the probe spacing; average convection time was divided into the probe spacing to yield the velocity. Probe spacings of 0.12 and 0.25 in. were used between adjacent probes; the outside probes were thus 0.37 in. apart. All three probe pairs were used to give values of convection velocity. Slight effects of aerodynamic interference were noticed at the closest spacing. At larger spacings, the greater effect of mixing compared to mean velocity than is encountered in most steady flows kept the aerodynamic interference from affecting the measurements.

In Fig. 7, the convection velocity results at Mach 9 are shown to agree with the previous anemometer measurements at Mach 6. Agreement is also shown with the prediction of the LHW theory for Mach 6 in air.[12-16] The axis velocity is shown from the LHW theory, while the probes are significantly off-axis compared with the wake width at low $X/D$; lower values of velocity than the axis prediction thus result at lower $X/D$. From the agreement at Mach 6 and Mach 9, it is concluded that the velocity does not change much with Mach number in this range.

In Fig. 8, the space correlation length scale $\Lambda$ is shown. The measured value of $\theta$, the time integral scale, was multiplied by the wake velocity $V$. This result is shown in Fig. 8 as "Taylor's hypothesis." Remarkable estimates were obtained by using a straight-line curve through unity at zero spacing and the averaged correlation value at the probe pair spacing. This estimating method was tested for the various shapes of correlation functions that have been measured,[17] and it was found to reproduce the integral value of $\Lambda$ within about 50% for most of the expected shapes. The fact that the two methods agree is interesting in

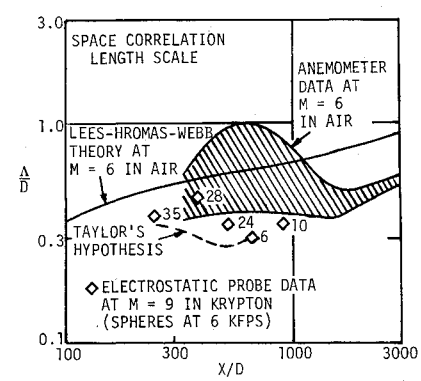


**Fig. 8 Space correlation length scale compared with Taylor's Hypothesis data and with anemometer data and also with Lees-Hromas-Webb theory.**

itself. Together, they show that the space correlation length scale of the electron density fluctuations at $M = 9$ agrees with the anemometer fluctuations space scale at $M = 6$ when $X/D \simeq 300$, but it is somewhat lower when $X/D \simeq 600$.

In Fig. 9, the time correlation integral scale $\theta$ is shown for the electron density fluctuations at $M = 9$ and compared with the anemometer results at $M = 6$. It may be worth renoting that the numbers next to the plotted values in the figures are the average basis; that is, the number of individual values that contribute to the average value that is plotted. The basis varied because of the varying signal-to-noise conditions.

The values of $\theta$ are shown in Fig. 9 to be nearly constant up to $X/D = 380$, including the measurement at $X/D = 100$ located on the edge of the wake. The electron density time scale $\theta$ at $M = 9$ agrees with the anemometer data scale $\theta$ at $M = 6$ when $X/D \simeq 300$. However, at $X/D \simeq 600$, the electron density scale is significantly lower. This effect appears to be related to the Mach number change between the two sets of data.

In a related paper on optical measurements,[18] the $X/D$ region near 600 has been shown to be the region where breakthrough occurs. It seems reasonable to expect the sensitivity of $\theta$ in this region to flow condition changes because this is the region of maximum density difference between the axis and front of the turbulent wake.[18]

## Electron Density Fluctuation Spectra

The major results presented are the electron density fluctuation spectra, which appear in this section. It is believed that these fluctuation spectra are the first available for electron density measurements in projectile wakes.

In Fig. 10, the spectra are shown for six analysis locations, namely, $X/D = 98$, 245, 380, 525 and 660. The power spectrum values are given as a ratio $P(f)/P(0)$, which is normalized by the value at zero frequency. The frequency scale is shown for just one value of $X/D$, namely, 98. The spectra for greater $X/D$ locations are shown on a shifted scale basis, that is, the displays are shifted for each spectrum. Instead of showing all of five scales, the individual spectrum data are identified by their frequency value. For example, the five values of $P(f)/P(0)$ that were all obtained at $f = 2.5$ kHz, but at different $X/D$, are joined by straight lines. If all of these data were plotted according to the single scale shown, they all would appear above or below the first value for $X/D = 98$.

Because the line joining the $P(2.5)/P(0)$ values in Fig. 10 generally rises with increasing $X/D$, it shows that an increasing power ratio was obtained at 2.5 kHz as $X/D$ increased. Likewise, from the slopes of the lines for $p(5.0)/P(0)$ and $P(7.5)/P(0)$, there is seen to be a sharp peak in power ratio at these frequencies when $X/D = 525$. It will be shown in later figures that many of these changes are due to the changes of scale $\theta$ that were noted in Fig. 9.

The average basis is also shown in Fig. 10. It indicates the number of individual spectra that contributed to the average

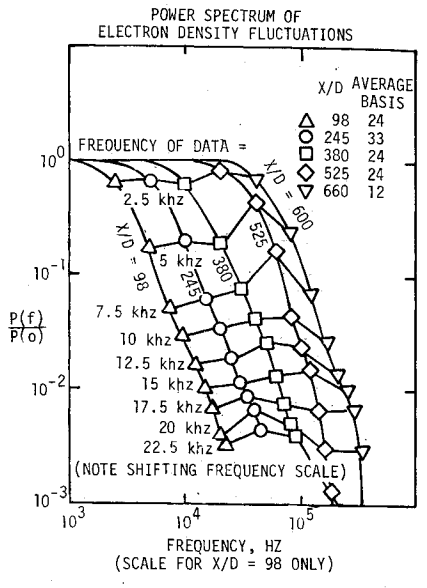


**Fig. 10 Power spectrum of electron density fluctuation using shifted scale for $X/D$ variation. Average basis for spectra are shown.**

spectrum for each $X/D$. An average basis of 33, for example, indicates that 11 shots were available with one spectrum from each of the probes and that all 33 spectra were averaged on a frequency-by-frequency basis to produce the average spectrum.

After averaging, each of the average data-plus-noise spectra were improved by subtracting an average noise spectrum from them. This noise spectrum was compiled from 24 spectra obtained by analyzing noise records before the projectile. The improvement was most noticeable at the last three frequencies, $f = 17.5$, 20, and 22.5 kHz. There, the low-data power made the noise power removal a significant improvement in data power trends.

It should be noted that the decrease of power ratio at high frequency with increasing $X/D$ that is seen in Fig. 10, is consistent with the idea of turbulent viscous dissipation occurring first in the smaller eddies. These small eddies contain the steepest instantaneous gradients which cause the most rapid decay of fluctuating energy. A measure of these smaller eddies, which is the microscale $\tau$, will be shown in a later figure.

Figure 11 shows the electron density spectra for $M = 9$, together with anemometer data spectra for $M = 6$. These anemometer spectra were produced from the data from a previous publication,[7] but they were only recently compiled into average spectra. Fifteen shots were used with two anemometer probes measuring the wake velocity and mass density fluctuations on each shot.

The spectra in Fig. 11 are displayed in two groups, $X/D \simeq 300$ and $X/D \simeq 600$. Individual frequency scales are provided for the two groups. At $X/D \simeq 300$, the two spectra at $M = 9$ agree well with the $M = 6$ spectrum. Because the wake velocity can be expected to change little with Mach number in this range, as shown in Fig. 7, certain conclusions can be drawn from the agreement between the anemometer and electron density spectra at $X/D \simeq 300$. The agreement between the values of $\theta$ at this $X/D$, as shown in Fig. 9, as well as the velocity and the spectral shape shows that the fluctuations are the same with respect to turbulent structure. Since the anemometer measures the mass velocity and mass density fluctuation field, the agreement with the electron density fluctuation field suggests that the electron density fluctuations are acting as a passive scalar embedded in the velocity and mass density fluctuation field.

At $X/D \simeq 600$, the spectra in Fig. 11 are separated for the two electron density fluctuation spectra and the single anemometer spectrum. This separation will be shown in the next figure to be mainly due to a change in scale $\theta$ or $\Lambda$ with changing Mach number. It may be noted in passing that the spectra are steeper than the $-\frac{5}{3}$ slope over most of the frequency range.

Figure 12 shows the same data and grouping as that displayed in Fig. 11; the only change is the normalization of the frequency scale with $\theta$, the time correlation integral scale. This normalization produces a close agreement for the high power ratio fluctuations at $X/D \simeq 600$ where a wide disagreement existed without this normalization. For the low-power ratio fluctuations at the higher frequencies, the scatter is about the same.

At $X/D \simeq 600$, the velocity is essentially the same for all three spectra, as shown in Fig. 7. The implication through Taylor's hypothesis is that the agreement on a normalized frequency basis of Fig. 12 is suggesting a rather strong change in scale $\theta$ or $\Lambda$ with Mach number. Since this is the breakthrough region of the viscous wake where it completely engulfs the hot inviscid wake, it is reasonable to expect sensitive response of the turbulent structure to changing flow conditions. It does seem remarkable that the large-power energy containing eddies scale as well as they do in Fig. 12 with $\theta$ or $\Lambda$. This agreement in shape of the high-power spectrum suggests a more rapid response of the large eddies than the small ones to changing flow conditions.

The normalization at $X/D \simeq 300$ in Fig. 12 produces slight

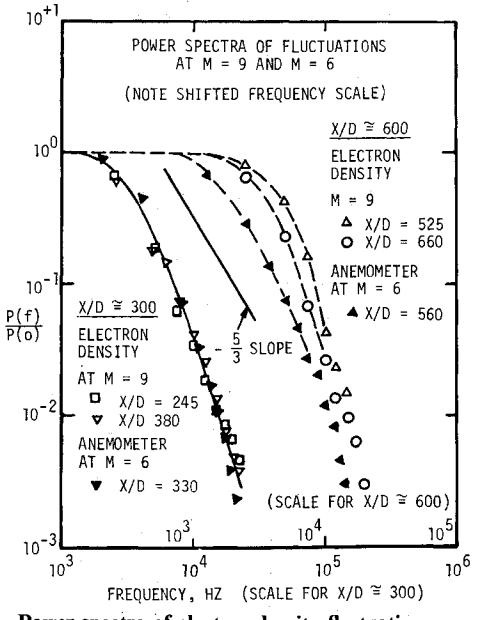


**Fig. 11 Power spectra of electron density fluctuations compared with anemometer data fluctuations for $X/D = 300$ and 600 using shifted scale.**

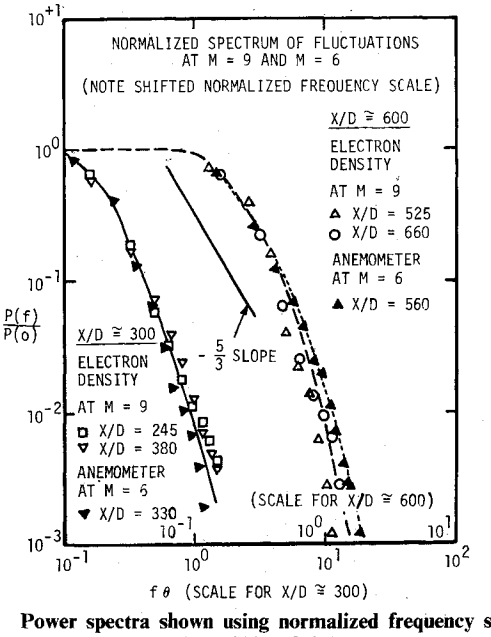


**Fig. 12 Power spectra shown using normalized frequency scales for $X/D = 300$ and 600.**

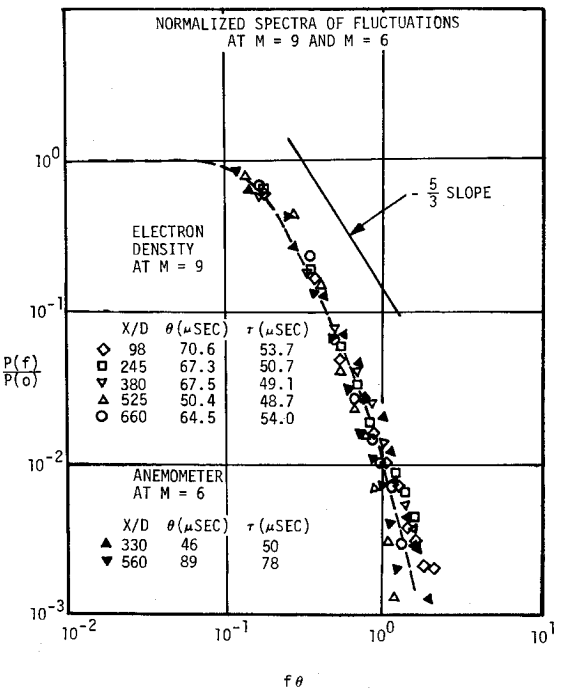


**Fig. 13 Normalized display of power spectra at $M = 6$ and $M = 9$ compared with $-\frac{5}{3}$ slope. Integral scales and microscales are listed.**

changes at high power and increases the scatter at low-power ratio compared with the frequency display of Fig. 11. To get better agreement, a two-scale normalization may be needed; this question will be examined in the next figure.

Figure 13 shows all of the previously displayed data from Fig. 12 using a single normalized frequency scale. In addition, the electron density fluctuation spectrum is shown from $X/D = 98$, which is the location of data taken at the edge of the wake. The agreement is excellent among all these spectra. The tabulated time correlation integral scales $\theta$ were calculated from the average spectra using the formula $\theta = P(0)/4(n_e')^2$ as before, and a similar formula for the anemometer data using the mean square data fluctuations instead of $(n_e')^2$.

The new scale $\tau$ shown in Fig. 13 is called the microscale because it measures the small scale fluctuations. It was calculated from the same formula that was used in previous publications[17]

$$\tau = [2\pi^2 \int f^2 P(f)\,df/(n_e')^2]^{-1/2} \qquad (6)$$

The microscale measures the power in the small fluctuations. For larger power in the small fluctuations, $\tau$ is small; the reverse is true if there is little power in the small fluctuations. The $\tau$ and $\theta$ in Fig. 13 move in parallel to a large degree; specifically, $\tau$ is usually somewhat smaller than $\theta$. Occasionally, $\tau$ can get slightly larger than $\theta$ as in the anemometer data at $X/D = 330$. This reversal also occurs in the last stages of decay of classical grid turbulence where the viscous-dissipation eddies are becoming as large as the energy-containing eddies.

The comparison of the spectra in Fig. 13 with the $-\frac{5}{3}$ slope shows that the data have a steeper slope over most of the frequency range. This steeper slope is consistent with the trends available from classical velocity-field turbulence. There, the turbulence Reynolds number based on the large scale energy structure must be of the order $10^6$ to obtain the Kolmogoroff slope of $-\frac{5}{3}$ in the inertial subrange. In the typical projectile wake, Reynolds numbers of the order of $10^4$ are obtained. A classical fluctuation spectra with Reynolds number of $10^4$ has a curved shape and steeper slope not unlike those shown in Fig. 13.

## Conclusions

The Mach 9 wakes of sphere projectiles that were measured showed rms electron density fluctuations that were from 0.6 to 1.0 of the mean electron density. The wake lasted for about 800 diameters to the location where oxygen attachment cleaned up the electron wake. The third central moment of the wake data remained positive, indicating the positive skewness or spikeyness of the data. Off-axis sensitivity was observed in the mean and rms electron density, but not in fluctuation intensity or spectra. The electron density fluctuation spectra, these being the first available, agree with anemometer spectra, suggesting that the electron density fluctuations are acting as a passive scalar embedded in the velocity and mass density fluctuation field. The measured spectra are steeper than the $-\frac{5}{3}$ slope over most of the frequency range. Although the velocity did not change much between the Mach 9 and Mach 6 data, a significant change of fluctuation scale was observed near breakthrough at $X/D \simeq 600$.

Progress on direct electron density fluctuation measurements at DREV is reported in Ref. 19.

## References

[1] Kornegay, W., "Electron Density Decay in Wakes," *AIAA Journal*, Vol. 3, No. 10, Oct. 1965, pp. 1819–1823.

[2] Hayami, R. A. and Primich, R. I., "Wake Electron Density Measurements Behind Hypersonic Spheres and Cones," AGARD Conference Proceedings No. 19 (Preprint), Fluid Physics of Hypersonic Wake Conference, Fort Collins, Colorado, May 1967.

[3] Cantin, A., Emond, A., and Heckman, D., "Observations on Electrostatic Probe Behavior in Ionized Turbulent Gas Flows in Ballistic Ranges," *International Congress on Instrumentation in Aerospace Facilities Proceedings*, IEEE Publication 69-C-19-AES, May 1969, pp. 20–33.

[4] French, I. P., Arnold, T. E., and Hayami, R. A., "Ion Distributions in Nitrogen and Air Wakes Behind Hypersonic Spheres," AIAA Paper 70-87, New York, 1970.

[5] Fox, J., Webb, W. H., Jones, B. G., and Hammitt, A. G., "Hot-Wire Measurements of Wake Turbulence in a Ballistic Range," *AIAA Journal*, Vol. 5, No. 1, Jan. 1967, pp. 99–102.

[6] Fox, J., "Space Correlation Measurements in the Fluctuating Turbulent Wakes Behind Projectiles," *AIAA Journal*, Vol. 6, No. 2, Feb. 1968, pp. 233–238; Rept. 07854-6021-R000, Feb. 1967, TRW Systems.

[7] Fox, J. and Rungaldier, H., "Anemometer Measurements of Velocity and Density in Projectile Wakes," *AIAA Journal*, Vol. 9, No. 2, Feb. 1971, pp. 270–276.

[8] Langmuir, I. and Mott-Smith, H. M., "The Theory of Collectors in Gaseous Discharges," *Physical Review*, Vol. 28, 1926, p. 727.

[9] Demetriades, A. and Doughman, E. L., "Langmuir Probe Diagnosis of Turbulent Plasmas," *AIAA Journal*, Vol. 4, No. 3, March 1966, pp. 451–459.

[10] Peterson, E. W. and Talbot, L., "Langmuir Probe Response in a Turbulent Plasma," AIAA Paper 69-698, San Francisco, Calif., 1969.

[11] Sutton, G. W., "Use of Langmuir Probes for Hypersonic Turbulent Wakes," *AIAA Journal*, Vol. 7, No. 2, Feb. 1969, pp. 193–199.

[12] Webb, W. H., "A Model for the Calculation of Radar Backscatter from Underdense Hypersonic Turbulent Wakes," Rept. 6433-6004-KU000, June 8, 1964, TRW Space Technology Lab.; also "Self-Preserving Fluctuations and Scales for the Hypersonic Turbulent Wake," *AIAA Journal*, Vol. 2, No. 11, Nov. 1964, pp. 2031–2033.

[13] Lees, L. and Hromas, L. A., "Turbulent Diffusion in the Wake of a Blunt Body at Hypersonic Speeds," Rept. 610-6005-MU000, July 1961, TRW Space Technology Labs.; also *Journal of the Aerospace Sciences*, Vol. 29, 1962, pp. 976–993.

[14] Webb, W. H. and Hromas, L. A., "Turbulent Diffusion of a Reacting Wake," *AIAA Journal*, Vol. 3, No. 5, May 1965, pp. 826–837.

[15] Hromas, L. A. and Lees, L., "Effect of Nose Bluntness on the Turbulent Hypersonic Wake," 6130-6259-KU000, Oct. 1962, TRW Space Technology Lab.

[16] Lees, L., "Hypersonic Wakes and Trails," ARS 17th Annual Meeting, Paper 2662-62, Nov. 1962; also *AIAA Journal*, Vol. 2, No. 3, March 1964, pp. 417–428.

[17] Hinze, J. O., *Turbulence*, McGraw-Hill, New York, 1959.

[18] Witte, A. B., Fox, J., and Rungaldier, H., "Localized Measurements of Wake Density Fluctuations Using Pulsed Laser Holographic Interferometry," AIAA Paper 70-727, San Diego, 1970.

[19] Staff of the Aerophysics Division, "Reentry Physics Research Program on Turbulent Wakes," DREV M-2122/71, June 1971, Defence Research Establishment Valcartier, Quebec, Canada.